scientific reports

OPEN

Dressed j_{eff}-1/2 objects in mixed-valence lacunar spinel molybdates

Thorben Petersen[1✉], Lilian Prodan[2], Korbinian Geirhos[2,3], Hiroyuki Nakamura[4], István Kézsmárki[2✉] & Liviu Hozoi[1✉]

The lacunar-spinel chalcogenides exhibit magnetic centers in the form of transition-metal tetrahedra. On the basis of density-functional computations, the electronic ground state of an Mo_4^{13+} tetrahedron has been postulated as single-configuration $a_1^2 e^4 t_2^5$, where a_1, e, and t_2 are symmetry-adapted linear combinations of single-site Mo t_{2g} atomic orbitals. Here we unveil the many-body tetramer wave-function: we show that sizable correlations yield a weight of only 62% for the $a_1^2 e^4 t_2^5$ configuration. While spin–orbit coupling within the peculiar valence orbital manifold is still effective, the expectation value of the spin–orbit operator and the g factors deviate from figures describing nominal $t^5 j_{eff} = 1/2$ moments. As such, our data documents the dressing of a spin–orbit $j_{eff} = 1/2$ object with intra-tetramer excitations. Our results on the internal degrees of freedom of these magnetic moments provide a solid theoretical starting point in addressing the intriguing phase transitions observed at low temperatures in these materials.

Mixed valency, the presence of more than one oxidation state for a particular chemical element, is associated with very rich physics, in both molecular and solid-state systems. It can be intrinsic, as for example in stoichiometric magnetite Fe_3O_4[1], or obtained through doping as in the colossal magneto-resistance manganese oxides $(R_{1-x}A_x)MnO_3$ (R = rare-earth cation, A = alkali or alkaline-earth cation)[2]. It can also imply quasi-localized ligand-hole states, i. e., ligand mixed valency, as shown for underdoped cuprates[3,4] or for the spin-Peierls compound NaV_2O_5[5,6]. Here we explore the mixed valence landscape in the molybdates $GaMo_4S_8$ and $GaMo_4Se_8$, lacunar-spinel quantum magnets displaying remarkable properties, e. g., modulated cycloidal and Néel-type skyrmion-lattice states with sub-10 nm periodicity that are coupled to ferroelectric polarization[7], a plethora of ferroelectric domain boundaries and junctions[8], and a cluster spin-glass phase[9]. Using advanced wave-function-based quantum chemical computational schemes, we show that the peculiar interplay of electronic correlations and spin–orbit interactions in these materials sets the stage for interesting physics and new insights: the dressing of a $j_{eff} = 1/2$ spin–orbit-coupled state[10] with virtual valence space excitations. This dressing, or correlation cloud, is evidenced with the help of wave-function analysis and of observables such as the ground-state g factors and branching ratios. The use of the latter as indicators for ground-state correlations is possible due to the presence of sizable spin–orbit interactions: in their absence, information can be obtained by comparing ab initio and experimental data for e. g. the cohesive energy[11,12]. The outcome of magnetization measurements performed on $GaMo_4S_8$ supports the computational findings and calls for spectroscopic verification of other specific predictions we make, e. g., of N-particle excitation energies as probed by resonant inelastic x-ray scattering experiments.

Results

High-temperature electronic structure, dressed $j_{eff} = 1/2$ states.
Spinels are generically described by the chemical formula AM_2X_4. The M sites define a pyrochlore lattice, each of those ions being encapsulated within an X_6 octahedral cage of nearest-neighbor chalcogenide ligands. Magnetite, for example, belongs to this class of systems, with Fe ions at both A and M sites[1]. In *lacunar* spinels, the A sites have half-integer occupation. With every second A cation removed, nearest-neighbor M_4 tetrahedra of the initial pyrochlore structure experience different surroundings; structural relaxation in the new setting yields a so called "breathing" pyrochlore

[1]Institute for Theoretical Solid State Physics, Leibniz IFW Dresden, Helmholtzstr. 20, 01069 Dresden, Germany. [2]Experimental Physics V, Center for Electronic Correlations and Magnetism, University of Augsburg, 86135 Augsburg, Germany. [3]Present address: Physik-Department, Technische Universität München, 85748 Garching, Germany. [4]Department of Materials Science and Engineering, Kyoto University, Kyoto 606-8501, Japan. ✉email: t.petersen@ifw-dresden.de; istvan.kezsmarki@physik.uni-augsburg.de; l.hozoi@ifw-dresden.de

lattice. The simplest way of representing that is as a *fcc* network of M_4 clusters (or of M_4X_{16} units), see Fig. 1a; adjacent M_4 entities share no M site.

Prior electronic-structure calculations based on density functional theory[13,14] point to a single-tetramer molecular-orbital-like diagram with a set of a_1, e, and t_2 levels at the top of the occupied orbital space, where the notations correspond to T_d point-group symmetry (see Fig. 1b). In $GaMo_4S_8$ and $GaMo_4Se_8$ there are formally 2.75 electrons per transition-metal (TM) site (i. e., $4 \times 2.75 = 11$ d electrons per Mo_4 cluster). Since the t_2 levels come at higher energy as compared to the a_1 and e components, the basic single-tetrahedron electronic structure in $GaMo_4X_8$ would then imply filled a_1 and e states and one hole within the t_2 sector. However, given the results of state-of-the-art quantum chemical calculations on related "clustered" compounds, both d-[15–18] and p-electron[19] based, there are reasons to believe that the picture presently put forward for the single-tetramer electronic structure in $GaMo_4X_8$ is somewhat too sketchy.

For insights into the *correlated* electronic structure of Mo_4^{13+} units in $GaMo_4S_8$ and $GaMo_4Se_8$, we adopt the embedded-cluster quantum chemical approach described in Ref.[18] and the lattice parameters and atomic positions determined by Powell et al. for $GaMo_4S_8$[20] and Routledge et al. for $GaMo_4Se_8$[21]. An $[Mo_4X_{16}]^{19-}$ cluster was in each case embedded within a large array of point charges created with the EWALD program[22,23]; capped effective core potentials (cECPs) were assigned to the 98 closest atoms. Further details on the embedding procedure are provided in the Supplemental Material (SM-1). The more general theoretical frame is mapped in Refs.[11,24].

The nature of the ground state and the low-energy excitation spectrum of a Mo_4 tetrahedron were first analyzed for the high-temperature (HT) structure, in both $GaMo_4S_8$ and $GaMo_4Se_8$. The leading ground-state configuration is $a_1^2 e^4 t_2^5 t_1^0 t_2^0$ (c.f. Figure 1b), but for a "converged" CAS(11e,12o) orbital space it comes with a weight of only 62% in the CASSCF ground-state wave-function (see Supplemental Material SM-3 for the active space orbitals and Supplementary Tables S1 and S2 in Supplemental Material SM-4 for the excited state configurations). The remaining configurations are mostly double excitations, e. g., $a_1^2 e^3 t_2^4 t_1^1 t_2^1$; there is a multitude of those, each contributing to the overall wave-function with a weight of less than 5%.

These findings do not seem unusual for this class of materials: important multiconfigurational effects, i. e., a weight of the $a_1^2 e^4 t_2^1$ leading electron configuration of less than 70%, were also found in the related 4d lacunar spinel $GaNb_4Se_8$[18]. The competition between different electronic configurations seems to be even sharper in the vanadium analogue[17,25].

Spin–orbit coupling (SOC) is effective for the multiconfigurational $^2T_2$ ground-state, giving rise to a low-lying spin–orbit doublet and a spin–orbit quartet with an excitation energy of about 0.12 eV (see Figs. 1b, 2). Yet, different from the $(\ldots a_1^2 e^4) t_2^5$ leading ground state configuration, unambiguously described in terms of $S = 1$, $L_{\text{eff}} = 1/2$, and $j_{\text{eff}} = 1/2$ quantum numbers[10], the multiconfigurational case entails more subtle nuances. This is discussed in the following paragraphs.

As depicted in Fig. 2, further excited states follow at energies exceeding 1 eV. Different from the ground $^2T_2$ term, spin–orbit interactions play a less important role for the higher-lying multiplets. But noticeable modifications occur post-CASSCF for the latter, at the NEVPT2 level; the sequence of the $^4A_2$ and $^2A_1$ terms, for instance,
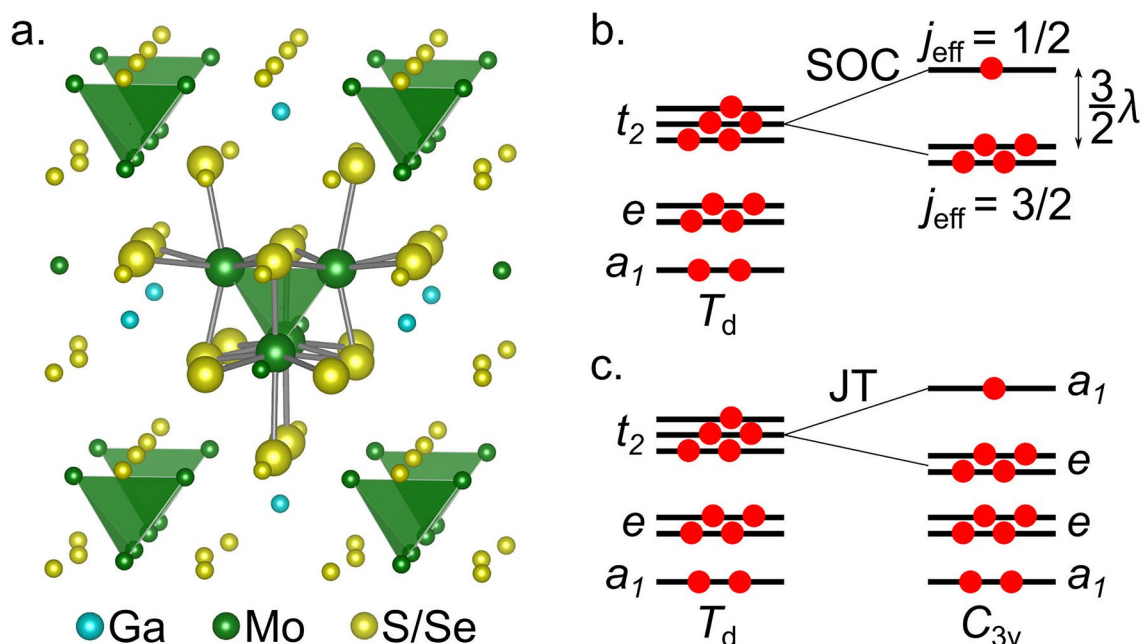

Figure 1. $GaMo_4X_8$ cluster model and molecular orbital schemes. (**a**) $GaMo_4S_8$/$GaMo_4Se_8$ cluster model. Mo_4 tetrahedra are shown in green. Small atomic spheres indicate capped effective core potentials (cECPs). (Ga: blue, Mo: green, S/Se: yellow). (**b**) Molecular-orbital diagram for the Mo_4 cluster in high-temperature, cubic T_d point group with spin–orbit coupling (SOC) and low-temperature, rhombohedral C_{3v} symmetry as a result of Jahn–Teller (JT) distortion.
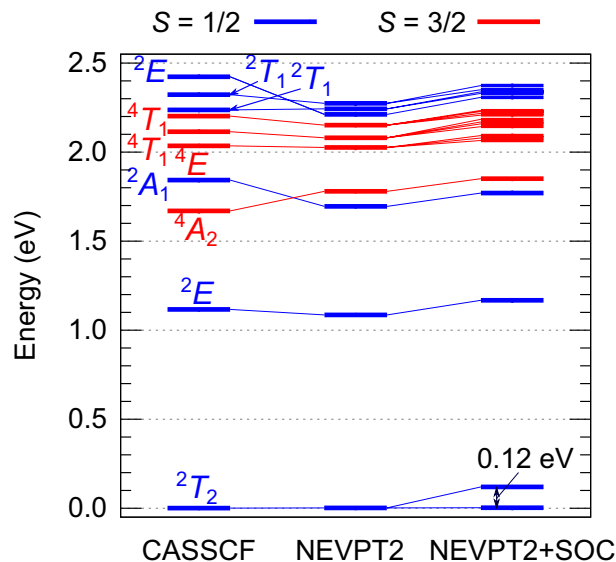
Figure 2. Low-energy excitation energies for high-temperature GaMo$_4$S$_8$. The spectrum was calculated using an [Mo$_4$S$_{16}$]$^{19-}$ embedded cluster model (CAS(11e,12o)). Both CASSCF and NEVPT2 values (also with SOC for the latter) are given in eV. Four quartets and six doublets were included in the state-averaging procedure. Notations according to T_d point group symmetry are used.

is different in NEVPT2 as compared to CASSCF. Comparing the NEVPT2 energies in GaMo$_4$S$_8$ and GaMo$_4$Se$_8$ (see Supplementary Material SM-4), it is seen that the excitation spectra are rather similar, somewhat scaled down in the latter compound. This can be attributed to having longer Mo-Se bonds in GaMo$_4$Se$_8$, i. e., weaker ligand fields.

To quantify the strength of spin–orbit interactions, the SOC constant λ was determined from minimal active space calculations. For such a CAS(5e,3o), which only incorporates the $(\dots a_1^2\, e^4)\, t_2^5$ configuration, the $j_{eff} = 3/2$ quartet is split by 100 meV from the $j_{eff} = 1/2$ ground-state term, yielding a SOC constant $\lambda_{SOC}^{Mo_4} = 67$ meV $= 538$ cm^{-1}. This value lies close to the SOC constant estimated for the $(\dots a_1^2\, e^4)\, t_2^1$ compound GaNb$_4$Se$_8$, $\lambda_{SOC}^{Nb_4} = 516$ cm^{-1}[18]. Compared to a Mo$^+$ single-ion value $\lambda_{SOC}^{Mo^+} = 630$ cm^{-1}[10], the SOC parameter is lower in GaMo$_4$Se$_8$, due to the more delocalized character of lacunar-spinel t_2 electrons – those orbit in lacunar spinels a four-site unit, not a single TM ion. The fact that the splitting between the lowest spin–orbit states increases when using larger active spaces (from 0.1 to 0.12 eV, see Fig. 2) has to do with electron correlations that bring in multiconfigurational physics; such effects were not addressed in earlier computations based on density functional theory[14,26].

A peculiar feature of nominal $j_{eff} = 1/2$ ground states is free-electron-like g factors[10], even if $L_{eff} = 1$. On the basis of the active space employed for the calculations [i. e., CAS(11e,12o)], ground-state g factors of 2.18 are obtained. The sizable deviation from 2 has to do with contributions of other electron configurations to the multiconfigurational ground-state wave-function, i. e., dressing with intra-tetramer excitations. For comparison, magnetic susceptibility measurements indicate a g value of 2.37 (see Supplementary Material SM-5). The somewhat larger experimental estimations hint towards additional vibronic effects[27,28] not included in the rigid cluster model.

Another quantity that can provide evidence for such dressing is the branching ratio (BR) in L-edge x-ray absorption spectroscopy (XAS), i. e., the ratio of the integrated intensities of the L_3 and L_2 absorption edges. It is directly related to the ground-state expectation value $\mathcal{Z}$ of the spin–orbit Hamiltonian and can be compactly expressed as BR $= (2 + r)/(1 - r)$[29–31], where $r = \mathcal{Z}/n_h$, n_h is the number of holes in the valence shell, and for a given LS term $\mathcal{Z} = \lambda^{-1}\mathcal{H}_{SO} = \mathbf{L} \cdot \mathbf{S}$. $\mathcal{Z}$ can be alternatively written as[30–32]

$$\mathcal{Z} = \lambda^{-1}\left(E_{LS}^0 - E_{LSJ}^0\right), \tag{1}$$

where E_{LS}^0 and E_{LSJ}^0 are ground-state eigenvalues without and with SOC, respectively. E_{LSJ}^0 may depend on both first- and second-order SOCs.

As an example, for a nominal $j_{eff} = 1/2$ spin–orbit ground state in t_{2g}^5 iridates[33,34] ($n_h = 5$), values $\mathcal{Z} = 1$ and BR $= 2.75$ are expected[35,36]; in contrast, for vanishing valence-shell spin–orbit interactions, $\mathcal{Z} \to 0$ and BR $\to 2$ are obtained. For the lacunar-spinel molybdates, using the minimal active space in the CASSCF calculation (five electrons within the three t_2 cluster orbitals), we find indeed $\mathcal{Z} = 1$ (see Table 1, first line). Slight reduction of the NEVPT2 minimal-CAS $\mathcal{Z}$ to 0.99 indicates the admixture of other electron configurations in the NEVPT2 treatment. Proper description of multiconfigurational physics requires however larger active spaces: enlarging the active space to CAS(11e,12o), $\mathcal{Z}$ increases to 1.2–1.3, even when only the lowest-lying $^2T_2$ term is included in the spin–orbit part of the computation. The difference between the large-CAS $\mathcal{Z}, \approx 1.2$, and the minimal-CAS $\mathcal{Z}$ of 1 is an indicator for the amount of dressing of the $j_{eff} = 1/2$ object with intra-tetramer electronic excitations. Interestingly, while in e. g. t_{2g}^5 iridates or rhodates this difference mainly arises from strong second-order

Number of states	Active space	$[Mo_4S_{16}]^{19-}$		$[Mo_4Se_{16}]^{19-}$	
		CASSCF	PT2	CASSCF	PT2
1D ($^2T_2$)	CAS(5e,3o)	1.00	0.99	1.00	0.99
1D ($^2T_2$)	CAS(11e,12o)	1.28	1.27	1.26	1.22
6D, 4Q	CAS(11e,12o)	1.26	1.23	1.25	1.22

Table 1. $\mathcal{Z}$ values in $GaMo_4S_8$ and $GaMo_4Se_8$. The $\mathcal{Z}$ values are given for different types of reference active spaces and different number of states in the spin-orbit treatment. The abbreviations refer to doublet (D) and quartet (Q) states. PT2 stands for NEVPT2.

SOCs[32,35,36], here those are inactive at HTs. $\mathcal{Z}$ being smaller and n_h larger than in t_{2g}^5 iridates, the BR is expected to be less than ≈ 2.5 in the molybdate lacunar spinels, which can be verified by XAS measurements.

Low-temperature electronic structure, $\tilde{S} = 1/2$ pseudo-spins. At temperatures of about 50 K, the $GaMo_4X_8$ lacunar spinels undergo a phase transition from cubic ($F\bar{4}3m$) to rhombohedral ($R3m$) space group[13], with compression of the $[Mo_4X_4]^{5+}$ tetrahedra along the cubic [111] direction, i. e., along a line connecting opposite Mo and X vertices[13,37,38]. This polar distortion gives rise to axial magnetic anisotropy along [111]. The effects of structural distortions as reported by Powell et al. for $GaMo_4S_8$[20] and by Routledge et al. for $GaMo_4Se_8$[21] were analyzed on the basis of CASSCF + NEVPT2 computations and orbital active spaces as employed for the HT phase (see Fig. 3 for $GaMo_4S_8$ and Supplementary Material SM-4 for $GaMo_4Se_8$).

Trigonal crystal-field splittings as large as 0.33 eV and 0.24 eV for $GaMo_4S_8$ and $GaMo_4Se_8$, respectively, are found to occur within the t_2 manifold, as illustrated by the splitting of the HT ground $^2T_2$ state into $^2A_1$ and ^2E terms. Obviously, this renders the $j_{eff} = 1/2$ picture inadequate. Yet, the effect of SOC is not negligible—three distinct Kramers doublets are found in the spin–orbit calculations, with relative NEVPT2 energies of 0, 0.32/0.23, and 0.38/0.29 eV. From a magnetic point of view, the pertinent effective picture for the Mo_4 tetrahedra is therefore that of $\tilde{S} = 1/2$ moments with significant angular-momentum contribution, in accordance with susceptibility measurements[39]. This is further seen in the structure of the ab initio low-T (LT) g factors (Table 2), where $g_{||}$ and $g_\perp$ refer to directions parallel and perpendicular to the rhombohedral axis (the [111] axis in cubic setting), respectively. A similar relation, $g_{||} < g_\perp$, was found for positive trigonal/tetragonal splittings in $RuCl_3$[40] and Ba_2IrO_4[32,41].

In order to experimentally verify the predicted type of axial anisotropy, characterized by $g_{||}/g_\perp < 1$, we measured the magnetization of LT $GaMo_4S_8$ along two non-equivalent directions, the [110] and [100] axes shown in Fig. 4. The [110] direction is perpendicular to the [111] rhombohedral axis, hence the corresponding saturation magnetization directly yields $g_\perp^{exp}$. Measurements with field applied along the [100] axis yield a combination of g factors, namely $\sqrt{g_{||}^2 \cos^2(54.7°) + g_\perp^2 \sin^2(54.7°)}$. Below 2 T, the low-temperature phase of $GaMo_4S_8$ shows a sequence of meta-magnetic transitions between different modulated magnetic states, including the skyrmionic lattice state[7], which is evidenced by anomalies in this region. These magnetic states are not the focus of the present work; instead, we study the high-field magnetization, with special emphasis on the anisotropy of the saturation
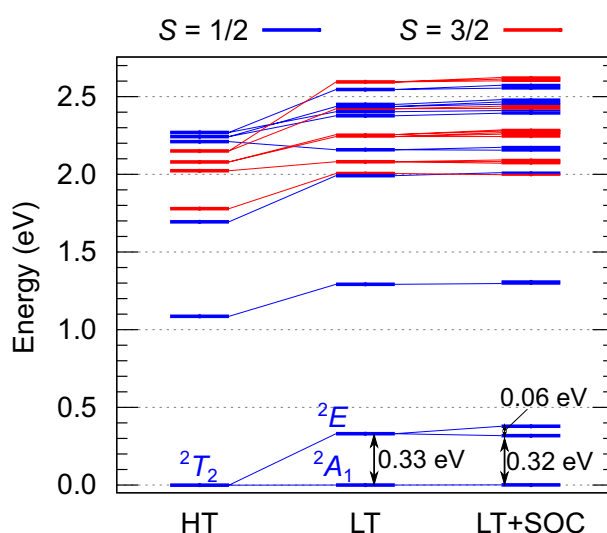

Figure 3. Influence of Jahn–Teller distortion on the low-energy excitation spectrum of $GaMo_4S_8$. Both high-temperature (HT) and low-temperature (LT) energies are given for the $[Mo_4S_{16}]^{19-}$ cluster model (NEVPT2(11e,12o)), including SOC for the latter. Six quartets and ten doublets were included in the state-averaging procedure.

Method	LT [Mo$_4$S$_{16}$]$^{19-}$		LT [Mo$_4$Se$_{16}$]$^{19-}$	
	$g_{\|\|}$ [a]	$g_\perp$	$g_{\|\|}$ [a]	$g_\perp$
CASSCF	1.87	2.43	1.76	2.56
NEVPT2	1.80	2.53	1.56	2.69
Exp.		2.54		

Table 2. Calculated g factors for LT [Mo$_4$X$_{16}$]$^{19-}$ (X = S, Se) cluster models (CAS(11e,12o)). [a]$g_{\|\|}$ refers to the cubic [111] axis (see also Fig. 4).
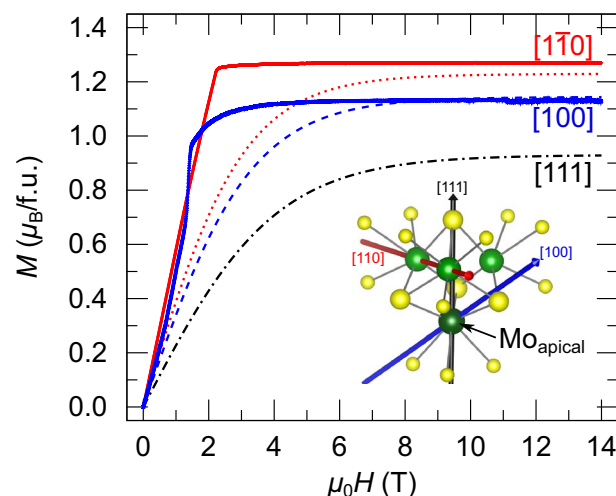
Figure 4. Magnetization curves for LT GaMo$_4$S$_8$. Measured (thick full lines) and simulated (dashed lines) curves were obtained at a temperature of 2.5 K. [1$\bar{1}$0] (red), [100] (blue), and [111] (black) directions are given in the cubic setting. The simulated curve is obtained for a [Mo$_4$S$_{16}$]$^{19-}$ embedded cluster (CASSCF(11e,12o)).

magnetization μ_{sat}. That allows us to determine the anisotropy of the g tensor. For both field directions, the measured magnetization is clearly saturated above ≈ 6 T. We find a tiny ($\approx 1\%$) decrease of the magnetization at higher fields, originating from a small diamagnetic contribution of the sample holder. This is visible only when the magnetization of the crystal is fully saturated.

For comparison, magnetization curves computed on the basis of the CASSCF(11e,12o) g factors[42] are also shown. At low fields between 1 and 4 T the simulated curves underestimate the measured magnetization, likely because of the single-tetrahedron model for which inter-tetrahedral magnetic interactions are absent. However, the experimental and simulated saturation magnetization values are in good agreement above 6 T, with $\mu_{sat}^{[110]} = 1.27\mu_B$ and $\mu_{sat}^{[100]} = 1.12\mu_B$. Since our calculated values are fully ab initio (with no ad hoc parameters in the underlying theory), small deviations can be assigned to structural differences present in experiment and embedded-cluster computations (see Supplemental Material SM-6).

Conclusions

With the help of ab initio quantum chemical calculations for both high- and low-temperature structural configurations, we shed light onto the nature of magnetic moments in mixed valence GaMo$_4$S$_8$ and GaMo$_4$Se$_8$. The quantum chemical computational data is referenced against low-temperature magnetization measurements. Our study documents the dressing of a bare $j_{eff} = 1/2$ object[10] with valence space excitations. We analyzed in this regard the wave-function itself and observables such as the ground-state g factors and the so-called branching ratios. The essential physics refers to genuine electron correlation effects, different from the case of layered t_{2g}^5 iridium oxides[33,34] where the branching ratios and ground-state g factors deviate from values corresponding to nominal $j_{eff} = 1/2$ moments due to j_{eff} 1/2–3/2 mixing and second-order spin–orbit couplings in the presence of lower-symmetry crystal/ligand fields[32,41]. The dressing, or correlation cloud, evidenced here has to do with the ground state of a Mo$_4$ tetramer, different from the quasiparticle concept utilized for excitations in solids. Its internal degrees of freedom determine the polar properties of the material, although a comprehensive description requires additionally an adequate treatment of vibronic couplings and inter-tetramer interactions.

Methods

All calculations were performed with the ORCA program package, v5.0[43]. Near-degeneracy correlation effects were accounted for by complete active space self-consistent field (CASSCF) theory[44,45] while additional dynamical correlations were described by N-electron valence second-order perturbation theory (NEVPT2)[46]. In the framework of the Douglas-Kroll-Hess (DKH) approximation[47], the all-electron SARC-DKH-TZVPP[48] basis set

for Mo and the DKH-DEF2-TZVPP[49] basis set for S/Se were used to treat SOC. To the cECPs, pseudopotentials of Andrae et al.[50] for Mo, Bergner et al.[51] and Leininger et al.[52] for Ga and S/Se were assigned. Additional computational details are given in the Supplemental Material (SM-2). For direct connection with experimental results, the magnetization of a $GaMo_4S_8$ single crystal grown by the flux method[53] was measured at 2.5 K in fields up to 14 T using a Quantum Design MPMS3.

Data availability

The datasets generated during and/or analysed during the current study are available from the corresponding author on reasonable request.

References

1. Attfield, J. P. Magnetism and the Trimeron Bond. *Chem. Mater.* **24**, 2877 (2022).
2. Coey, J. M. D., Viret, M. & von Molnár, S. Mixed-valence manganites. *Adv. Phys.* **48**, 167 (1999).
3. Zhang, F. C. & Rice, T. M. Effective Hamiltonian for the superconducting Cu oxides. *Phys. Rev. B* **37**, 3759 (1988).
4. Hozoi, L. *et al.* Quasiparticle bands in cuprates by quantum chemical methods: Towards an ab initio description of strong electron correlations. *Phys. Rev. Lett.* **99**, 256404 (2007).
5. Hozoi, L. *et al.* Theoretical characterization of the ground and optically excited states of α'-NaV$_2$O$_5$. *Phys. Rev. Lett.* **89**, 076407 (2002).
6. Hozoi, L., Nishimoto, S. & Yamasaki, A. Near degeneracy and pseudo Jahn-Teller effects in mixed-valence ladders: The phase transition in NaV$_2$O$_5$. *Phys. Rev. B* **72**, 195117 (2005).
7. Butykai, A. *et al.* Squeezing the periodicity of Néel-type magnetic modulations by enhanced Dzyaloshinskii-Moriya interaction of 4d electrons. *npj Quantum Mater.* **7**, 1 (2022).
8. Neuber, E. *et al.* Architecture of nanoscale ferroelectric domains in GaMo$_4$S$_8$. *J. Phys. Condens. Matter.* **30**, 445402 (2018).
9. Malta, J. F., Henriques, M. S. C., Paixão, J. A. & Gonçalves, A. P. Evidence of a cluster spin-glass phase in the skyrmion-hosting GaMo$_4$S$_8$ compound. *J. Mater. Chem. C* **10**, 12043 (2022).
10. Abragam, A. & Bleaney, B. *Electron Paramagnetic Resonance of Transition Ions* (Clarendon Press, 1970).
11. Fulde, P. *Correlated Electrons in Quantum Matter* (World Scientific, 2012).
12. Yang, J. *et al.* Ab initio determination of the crystalline benzene lattice energy to sub-kilojoule/mole accuracy. *Science* **345**, 640 (2014).
13. Pocha, R., Johrendt, D. & Pöttgen, R. Electronic and Structural Instabilities in GaV$_4$S$_8$ and GaMo$_4$S$_8$. *Chem. Mater.* **12**, 2882 (2000).
14. Lee, H. *et al.* Charge density functional plus U calculation of lacunar spinel GaM$_4$Se$_8$ (M = Nb, Mo, Ta, and W). *Europhys. Lett.* **125**, 47005 (2019).
15. Majumdar, D. & Balasubramanian, K. Theoretical study of the electronic states of Nb$_4$, Nb$_5$ clusters and their anions (Nb$_4^-$, Nb$_5^-$). *J. Chem. Phys.* **121**, 4014 (2004).
16. Sharma, S., Sivalingam, K., Neese, F. & Chan, G.K.-L. Low-energy spectrum of iron–sulfur clusters directly from many-particle quantum mechanics. *Nat. Chem.* **6**, 927 (2014).
17. Hozoi, L., Eldeeb, M. S. & Rößler, U. K. V$_4$ tetrahedral units in AV$_4$X$_8$ lacunar spinels: Near degeneracy, charge fluctuations, and configurational mixing within a valence space of up to 21 d orbitals. *Phys. Rev. Res.* **2**, 022017(R) (2020).
18. Petersen, T. *et al.* How correlations and spin-orbit coupling work within extended orbitals of transition-metal tetrahedra of 4d/5d lacunar spinels. *J. Phys. Chem. Lett.* **13**, 1681 (2022).
19. Petersen, T., Rößler, U. K. & Hozoi, L. Quantum chemical insights into hexaboride electronic structures: Correlations within the boron p-orbital subsystem. *Commun. Phys.* **5**, 214 (2022).
20. Powell, A. V. *et al.* Cation substitution in defect thiospinels: Structural and magnetic properties of GaV$_{4-x}$Mo$_x$S$_8$ (0≤x≤4). *Chem. Mater.* **19**, 5035 (2007).
21. Routledge, K. *et al.* Mode crystallography analysis through the structural phase transition and magnetic critical behavior of the lacunar spinel GaMo$_4$Se$_8$. *Chem. Mater.* **33**, 5718 (2021).
22. Klintenberg, M., Derenzo, S. & Weber, M. Accurate crystal fields for embedded cluster calculations. *Comp. Phys. Commun.* **131**, 120 (2000).
23. Derenzo, S. E., Klintenberg, M. K. & Weber, M. J. Determining point charge arrays that produce accurate ionic crystal fields for atomic cluster calculations. *J. Chem. Phys.* **112**, 2074 (2000).
24. Fulde, P. Wavefunctions of macroscopic electron systems. *J. Chem. Phys.* **150**, 030901 (2019).
25. Petersen, T., Rößler, U. K. & Hozoi, L. Luxuriant correlation landscape in lacunar spinels: multiconfiguration expansions in molecular-orbital basis vs resonant valence structures. arXiv:2301.03392 (2023)
26. Kim, H.-S., Im, J., Han, M. J. & Jun, H. Spin-orbital entangled molecular j$_{eff}$ states in lacunar spinel compounds. *Nat. Commun.* **5**, 3988 (2014).
27. Faughnan, B. W. Electron-paramagnetic-resonance spectrum of Mo^{5+} in SrTiO$_3$ – an example of the dynamic Jahn-Teller effect. *Phys. Rev. B* **5**, 4925 (1972).
28. Kahn, O. & Kettle, S. Vibronic coupling in cubic complexes. *Mol. Phys.* **29**, 61 (1975).
29. Thole, B. T. & van der Laan, G. Linear relation between x-ray absorption branching ratio and valence-band spin-orbit expectation value. *Phys. Rev. A* **38**, 1943 (1988).
30. Thole, B. T. & van der Laan, G. Branching ratio in x-ray absorption spectroscopy. *Phys. Rev. B* **38**, 3158 (1988).
31. van der Laan, G. Spin-orbit branching ratio and magnetic x-ray dichroism. *Phys. Scr.* **41**, 574 (1990).
32. Katukuri, V. M. *et al.* Electronic structure of low-dimensional 4d^5 oxides: Interplay of ligand distortions, overall lattice anisotropy, and spin-orbit interactions. *Inorg. Chem.* **53**, 4833 (2014).
33. Kim, B. J. *et al.* Phase-sensitive observation of a spin-orbital Mott state in Sr$_2$IrO$_4$. *Science* **323**, 1329 (2009).
34. Jackeli, G. & Khaliullin, G. Mott insulators in the strong spin-orbit coupling limit: From Heisenberg to a quantum compass and Kitaev models. *Phys. Rev. Lett.* **102**, 017205 (2009).
35. Laguna-Marco, M. A. *et al.* Orbital magnetism and spin-orbit effects in the electronic structure of BaIrO$_3$. *Phys. Rev. Lett.* **105**, 216407 (2010).
36. Haskel, D. *et al.* Pressure tuning of the spin-orbit coupled ground state in Sr$_2$IrO$_4$. *Phys. Rev. Lett.* **109**, 027204 (2012).
37. Reschke, S. *et al.* Lattice dynamics and electronic excitations in a large family of lacunar spinels with a breathing pyrochlore lattice structure. *Phys. Rev. B* **101**, 075118 (2020).
38. Geirhos, K. *et al.* Optical, dielectric, and magnetoelectric properties of ferroelectric and antiferroelectric lacunar spinels. *Phys. Status Solidi B* **259**, 2100160 (2021).

6

39. Malik, V., Yadav, C. S., Rastogi, A. & Kumar, D. Peculiar magnetism of transition metal cluster compounds. *Europhys. Lett.* **101**, 67008 (2013).
40. Yadav, R. *et al.* Kitaev exchange and field-induced quantum spin-liquid states in honeycomb α-RuCl₃. *Sci. Rep.* **6**, 37925 (2016).
41. Bogdanov, N. *et al.* Orbital reconstruction in nonpolar tetravalent transition-metal oxide layers. *Nat. Commun.* **6**, 7306 (2015).
42. Chibotaru, L. & Ungur, L. Ab initio calculation of anisotropic magnetic properties of complexes: I: Unique definition of pseudospin Hamiltonians and their derivation. *J. Chem. Phys.* **137**, 064112 (2012).
43. Neese, F. Software update: The ORCA program system—Version 5.0. *WIREs Comput. Mol. Sci.* **12**, e1606 (2022).
44. Roos, B. O. The complete active space self-consistent field method and its applications in electronic structure calculations. In Adv. Chem. Phys. (Wiley, 1987) pp. 399–445.
45. Helgaker, T., Jørgensen, P. & Olsen, J. *Molecular Electronic-Structure Theory* (Wiley VCH, 2000).
46. Angeli, C., Cimiraglia, R., Evangelisti, S., Leininger, T. & Malrieu, J.-P. Introduction of n-electron valence states for multireference perturbation theory. *J. Chem. Phys.* **114**, 10252 (2001).
47. Dunning, T. H. Gaussian basis sets for use in correlated molecular calculations: I: The atoms boron through neon and hydrogen. *J. Chem. Phys.* **90**, 1007 (1989).
48. Rolfes, J. D., Neese, F. & Pantazis, D. A. All-electron scalar relativistic basis sets for the elements Rb–Xe. *J. Comput. Chem.* **41**, 1842 (2020).
49. Weigend, F. & Ahlrichs, R. Balanced basis sets of split valence, triple zeta valence and quadruple zeta valence quality for H to Rn: Design and assessment of accuracy. *Phys. Chem. Chem. Phys.* **7**, 3297 (2005).
50. Andrae, D., Häußermann, U., Dolg, M., Stoll, H. & Preuß, H. Energy-adjusted ab initio pseudopotentials for the second and third row transition elements. *Theoret. Chim. Acta* **77**, 123 (1990).
51. Bergner, A., Dolg, M., Küchle, W., Stoll, H. & Preuß, H. Ab initio energy-adjusted pseudopotentials for elements of groups 13–17. *Mol. Phys.* **80**, 1431 (1993).
52. Leininger, T. *et al.* Spin-orbit interaction in heavy group 13 atoms and TlAr. *Chem. Phys.* **217**, 19 (1997).
53. Querré, M. *et al.* Electric pulse induced resistive switching in the narrow gap Mott insulator GaMo₄S₈. *Key Eng. Mater.* **617**, 135 (2014).

Acknowledgements

Author contributions
T.P. carried out the quantum chemical calculations. L.P. and K.G. performed the magnetization measurements. H.N. synthesized the single crystals. T.P. and L.H. wrote the initial version of the manuscript in consultation with all authors. I.K. and L.H. planned and supervised the project.

Funding

Competing interests
The authors declare no competing interests.

Additional information
Supplementary Information The online version contains supplementary material available at https://doi.org/10.1038/s41598-023-28656-3.

Correspondence and requests for materials should be addressed to T.P., I.K. or L.H.

Reprints and permissions information is available at www.nature.com/reprints.

Publisher's note Springer Nature remains neutral with regard to jurisdictional claims in published maps and institutional affiliations.